25th ABCM International Congress of Mechanical Engineering
October 20-25, 2019, Uberlândia, MG, Brazil

COB-2019-1971
INFLUENCE OF COPPER FOAM THICKNESS ON POOL BOILING OF HFE-7100

Leonardo Lachi Manetti, leonardo.manetti@unesp.br
Reinaldo Rodrigues de Souza, reisartre@gmail.com
Elaine Maria Cardoso, elaine.cardoso@unesp.br
UNESP – Universidade Estadual Paulista "Júlio de Mesquita Filho", Faculdade de Engenharia de Ilha Solteira, Av. Brasil Centro, 56, Departamento de Engenharia Mecânica, M4, 15385-000, Ilha Solteira, SP

Abstract. *Pool boiling is a low-cost technique for cooling electronic devices; HFE-7100 is a dielectric fluid with advantageous properties for such application however, it can cause a temperature overshoot in the system. Hence, the use of porous heating surface improves the heat transfer performance, eliminating the temperature overshoot due to their interconnected porous, which increase the wet area and active nucleation site density. In this work, we carried out pool boiling tests by using HFE-7100 and copper foams at three different thicknesses: 3 mm, 2 mm, and 1 mm in order to study the vapor bubble dynamics into the foam cell and find out an optimum thickness to enhance the boiling heat transfer. The results show that high thickness, 2 mm and 3 mm, has the best performance at low heat fluxes while the lowest thickness has the best performance at high heat fluxes. At heat fluxes lower than 50 kW/m², the higher wet area increases the natural convection zone even though the latent heat also playing an important role. At higher heat fluxes, mainly after 200 kW/m², the vapor bubbles are trapped in the foam structure leading to an unstable boiling pattern with damage to the rewetting process. Therefore, lowest foam thickness reduces the entrapment of the vapor into the cell; additionally, the capillary-wicking ability increases, which improves the HTC and the liquid replenishment in the foam cell delaying the dryout occurrence.*

Keywords: *pool boiling, HFE-7100, porous surface, copper foam, thickness.*

1. INTRODUCTION

It is well known that microelectronics and microchips have been increasing in power, so in and heat generation also, but decreasing in size (Yang and Liu, 2018). Efficient thermal management solutions are crucial to maintaining new electronic devices within the operating temperature limits (Leong et al., 2017). Immersion cooling with two-phase change – pool boiling – is a low-cost technique because it works with passive fluid circulation and requires low maintenance. Consequently, pool boiling has been used as a way of reaching the power dissipation needed by electronic devices (El-Genk, 2012). Another pool boiling advantage is the component-liquid direct contact that eliminates the contact resistance; however, liquids with high electric conductive, *e.g.* water, cannot be used. For this reason, the fluorochemical fluids such as fluorocarbons (FCs) and hydrofluoroethers (HFEs) are advantageous due to their dielectric and inert properties, nonflammable and non-reactive characteristics, *i.e.* they are chemically compatible (Liang and Mudawar, 2019). Besides that, FC-72 and HFE-7100 have a low boiling point, $T_{sat} \approx 60$ °C at 1 atm, which maintains the electronic components at low operating temperatures, < 85 °C (Teodori et al., 2014); both of them are chlorine free fluid that provides an ozone depleting potential, ODP = 0; and, HFE-7100, has a superior environmental properties due to its global warming potential, $GWP_{100} = 320$ (3M Company, 2002) while FC-72 has a $GWP_{100} > 5000$ (3M Company, 2002).

Pool boiling system is limited by the critical heat flux (CHF) and the heat transfer coefficient (HTC) values caused by counter flow of vapor and liquid flow during the process (Khan et al., 2019). One promising way to enhance the CHF and the HTC is to modify the heating surface morphology (Seo et al., 2018). Porous surface structures have been widely reported to enhance heat transfer performance due to their interconnected porous, which increase the wet area and the nucleation site density (Shojaeian and Koşar, 2015). The porous thickness and pore size are the two important parameters of a porous surface, and their optimal values mainly depend on the fluid properties (Lin and Kedzierski, 2019). The open cell metal foams are surfaces with high porosity ($\varepsilon > 80\%$) composed by tetradecahedron foam cells (Gibson and Ashby, 1997). According to Zhao (2012), these metal foams have high surface area density (>1000 m²/m³) and low-cost manufacturing process.

Researchers have been studying experimental works in pool boiling by using metal foams. Atherya et al. (2002) studied FC-72 on aluminum metal foam with different thickness (2.3 mm – 25.4 mm) and different pores per inch (PPI).

As the heat flux increases, the bubbles within the structure also increase; thicker foams enhance the HTC at low heat fluxes values while the lowest thickness had the highest CHF.

Xu et al. (2008) used acetone as working fluid on copper foam with three different porous densities 30, 60, and 90 PPI at constant thickness (δ = 3 mm). All foams presented negligible wall temperature overshoot at boiling incipience. The authors reported a HTC and CHF enhancement due to the high liquid contact area, more density of active sites, and capillary-assist liquid flow towards foam cells. Yang et al. (2010) used the Xu et al. (2008) methodology and surfaces; however, they used water as working fluid and different foams thickness – from 1 mm to 5 mm. They found out that the HTC enhancement on the metal foams depends on the balance between the liquid suction capability towards the porous structure and the vapor release resistance to the bulk liquid. The optimum thickness decreases as the porous density increases because high porous density increases the surface area and, consequently, the nucleation sites; however, it decreases the bubbles release resistance.

Xu and Zhao (2013) investigated the pool boiling heat transfer of deionized (DI) water on a copper foam surface with V-shape grooves. They reported that large foam thickness can offer a high surface area although creates considerable resistance for bubble escape; thus, grooves in the foam structure could help the vapor bubbles escape. Additionally, Xu and Zhao (2015) studied DI water on pool boiling of gradient metal foams (foam of high porous density at the lower level and low porous density at the upper level). According to them, the low porous density delays the bubble departure and increases the bubble growing time, enhancing the HTC; and, the high density increases the nucleation sites.

Recently, Wong and Leong (2018) printed a homogeneous metal foam structure by using Selective Laser Melting (SLM) in order to study the effect of porous diameter and foam thickness on pool boiling of FC-72. They concluded that porous structures increase the bubble nucleation site density due to the larger surface area and capillary-assisted liquid suction which allow better liquid replenishment; however, a larger surface area corresponds to an increase in the form drag and, consequently, in the bubble evacuation resistance. The bubble evacuation resistance increases for higher heat flux, structure height and smaller unit cell size.

Based on the previous literature review, the metal foams increase the HTC and the CHF as compared to a plain/flat surfaces. The main effect is the wet area enhancement that promotes bubbles formation at low heat fluxes coupled with more nucleation sites as heat flux increases; moreover, the higher the foam PPI the larger the wet area and the smaller the pore diameter. Surfaces with small pores increase the capillary-assist liquid flow towards foam cells; however, small pores difficult the bubble vapor evacuation at high heat fluxes. Moreover, the higher the foam thickness the larger the wet area, improving the HTC at low heat fluxes (the opposite behavior is observed at high heat fluxes due to thermal resistance enhancement caused by the vapor within the porous structure).

In this paper, we present pool boiling experimental results by using HFE-7100 (at saturated conditions) on metal foams of copper (Cu) at three different thicknesses (δ): 3 mm, 2 mm, and 1 mm. The present work aims to: (i) increase the database of fluid-surface combinations; (ii) understand the vapor bubble dynamics into the foam cell by using high-speed camera images and liquid flow by wickability analysis; (iii) find an optimum foam thickness to enhance the boiling heat transfer.

2. SURFACE PREPARATION AND CHARACTERIZATION

2.1 Foams parameters

The porous surfaces were purchased from Nanoshel® in 500 × 500 mm^2 panels. They are open cell metal foam, with 3 mm thick, fabricated by using metal deposition in a cellular preform as detailed by Ashby et al. (2000) and Bahart (2001). They were cut in 16 × 16 mm^2 panels by using a wire electrical discharge machining (wire-EDM, Groover, 2012). The porosity (ε) was obtained by weighting seven samples with the same size in an analytical balance and comparing the foam density, ρ_{foam}, with the copper density,

$$\varepsilon = 1 - \rho_r = 1 - \frac{\rho_{foam}}{\rho_{Cu}} \tag{1}$$

Moreover, the following methods were used to characterize the copper foams (Fig. 1): (i) optical images by using a stereo microscopy Zeiss® SteREO Discovery.V8 and scanning electron microscopy (SEM) by using an EVO LS15 Zeiss®; (ii) X-ray microcomputed tomography (μCT) by using a Skycan 1272 at a resolution of 15 μm (100 kV X-ray source voltage); and, (iii) wickability based the wicked volume in a capillary tube (1 mm diameter).

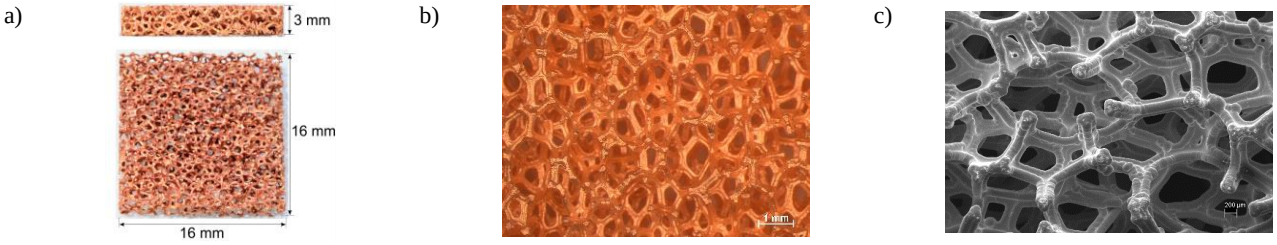

Figure 1. Copper foam: (a) entire section (b) stereo top view; (c) SEM top view.

In order to perform the PPI measurement, by using the Stereo images, seven lines in each direction were traced and the number of porous in which intercepted lines were counted; so, an average of the two direction yields the PPI of the open cell metal foam. The average PPI value was 31.75 with a standard deviation of 6.2. In addition, the µCT images were used for measuring the foam porous diameter and fibers diameters (d_p and d_f, respectively), and the specific area (a_{sf}). First, the µCT virtual slices were input in the Imoph software (Brun et al., 2008) in order to measure the surface granulometry by using the aperture map function for both phases (solid and porous), as explained by Vicente et al. (2006). Figure 2a shows the histogram and the normal distribution that permits to define a mean pore diameter (Tab. 1). The µCT virtual slices were input in the vmtk® software for measuring the specific area; vmtk uses the 'marching cubes' algorithm to extract the interface between the porous and solid phases by creating a triangulated surface mesh that is rendered to form a solid (Fig. 2b). A gray scale threshold value was selected such that the porosity of the reconstructed 3D volume matched with the measured foam porosity as explained by (Sarangi et al. 2017). After setting the correct gray scale, the area density was obtained by the ratio between the surface solid area (foam area) and its total volume (solid volume + porous volume).

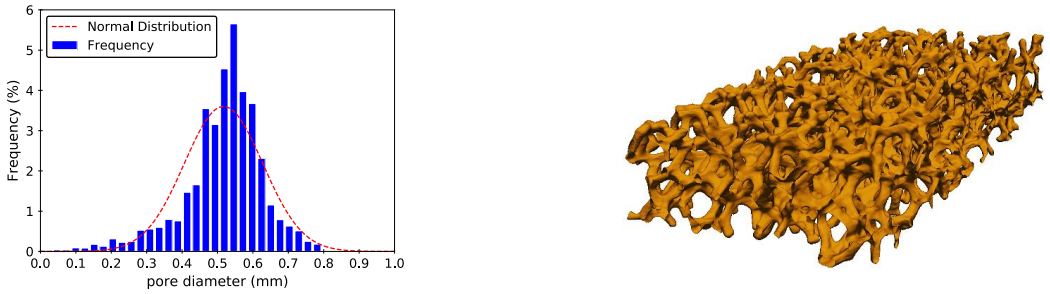

(a) (b)

Figure 2. Copper foam (a) pore diameter distribution; (b) rendered tridimensional surface.

Table 1. Copper foam characteristics.

Weight (kg×10^{-3})	ρ_{foam} (kg/m³)	ρ_r[1] (%)	ε (%)	d_p (mm)	d_f (mm)	a_{sf} (m^2/m^3)
0.697	908.1	10.1	90.0	0.52	0.1	2166

[1]Pure material density: ρ_{Cu} = 8960 kg/m³.

The metal foams with a thickness of 3 mm were welded on the copper block (Fig. 3a) using tin-lead (0.1 mm thickness) as solder, in order to ensure a low thermal resistance between the foam and the test section. Two other foam thicknesses were tested by using the electric discharge machining process (EDM) where a square flat copper block (20 × 20 mm^2) was used as electrode tool. Figure 3b shows the copper foam after the machining process, with δ =1 mm.

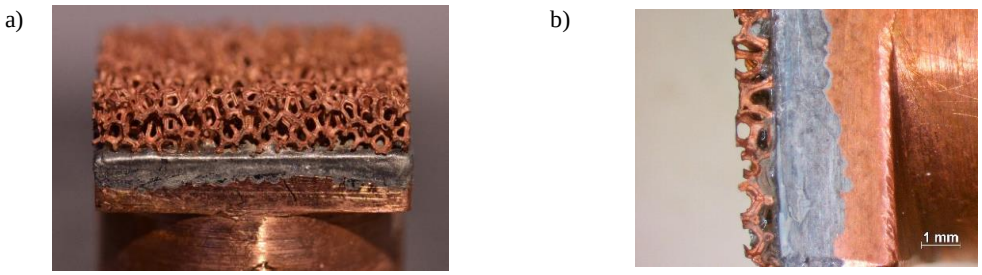

Figure 3. Copper foam welded on the copper block: (a) original, δ = 3 mm; (b) after machining process, δ = 1mm.

2.2 Wickability analysis

Previous works on metal foams (Xu et al., 2008; Yang et al. 2010; Xu and Zhao, 2013; Zhou et al. 2018) refer the capillary-assist as one of the main causes for the HTC and CHF enhancement. They based their analysis on Young-Laplace equation by considering the interconnected pores as capillary tubes; therefore, the smaller the pore diameter the larger the capillary driving pressure, which should improve the liquid replenishment (Zhou et al. 2018).

Ahn et al. (2012), Rahman et al. (2014), Cao et al. (2018) and Cao et al. (2019) carried out capillary-wicking test where the porous surface is slowly raised to contact a pendant fluid droplet attached to a small diameter capillary tube. As the surface contacts the liquid droplet, the fluid is wicked into the porous structure and the volumetric flow rate is measured by monitoring the liquid meniscus in the tube. The wickability is characterized by the absorbed flow rate defined as,

$$\dot{V} = A_c \left(\frac{dh}{dt}\right)_{t=0} \tag{2}$$

where A_c is the capillary tube area and dh is the liquid column variation inside the capillary tube.

The experimental layout is shown in Fig. 4a where the capillary tube had 1 mm in diameter and the liquid volume wicked by all surfaces tested is shown in Fig. 4b at the first 30 milliseconds (the straight lines represent the initial wicked volume). One may observe that the thinnest foam showed the best capillary wicking behavior.

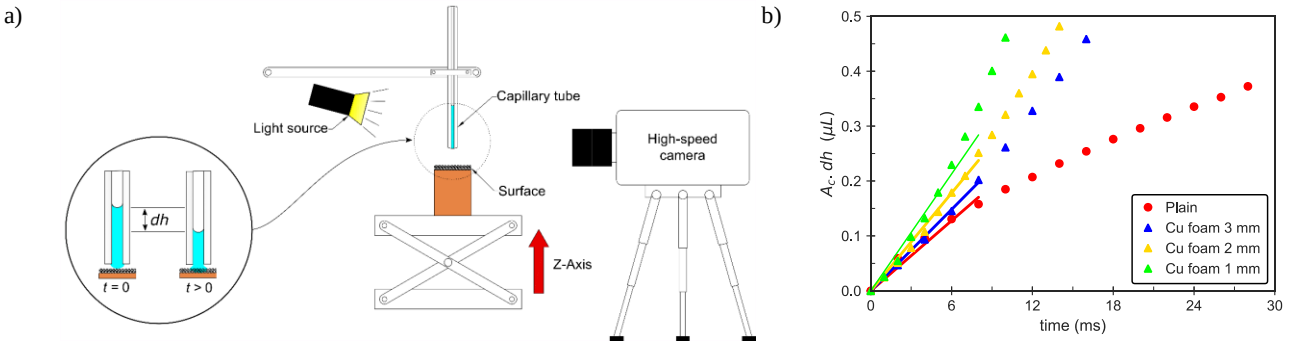

Figure 4. Wickability measurement: (a) Schematic layout experimental (b) Volume wicked by all surfaces tested.

3. EXPERIMENTAL SETUP AND DATA REDUCTION

Figure 5a shows the pool boiling apparatus, which consisted of a rectangular vessel made of glass with wall thickness of 5 mm. Water from a thermal bath circulated through a cooling coil located at the top of the boiling chamber. This heat exchanger was used to control the saturation pressure inside the vessel. An auxiliary heater – a cartridge resistance with a maximum power of 250 W at 220 V – submerged in the working fluid was used to maintain the liquid temperature near the saturation state. Two K-type thermocouples, T_{liq} and T_{vap}, located in the liquid and vapor regions of the vessel, respectively, were used to monitor the test fluid temperature. An absolute pressure transducer Omega PXM309-2A measured the pressure inside the boiling chamber. The experiments were performed under conditions close to the local atmospheric pressure, p_{atm} = 98 ± 0.05 kPa.

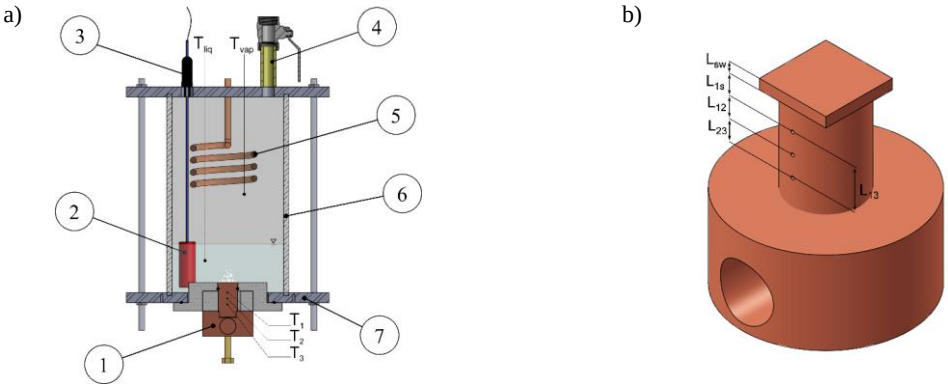

Figure 5. (a) Pool boiling apparatus: (1) cooper block; (2) auxiliary heater; (3) pressure transducer; (4) vacuum/feed valve; (5) condenser; (6) glass chamber; (7) stainless steel plate. (b) Test section view: (a) distance between the thermocouples and the surface.

The test section, Fig. 5b, consisted of a copper piece with a square face at the top surface (16 × 16 × 3 mm^3) on a copper block with 16 mm diameter and 60 mm height; three K-type thermocouples (T_1, T_2, and T_3) with 0.5 mm

diameters were used to estimate the wall temperature (T_w) and the heat flux ($q''_{measured}$). A cartridge resistance heated the bottom part of the copper block; power was supplied by a stabilized variable DC power source. The thermal insulation of the test section consisted of polytetrafluoroethylene (PTFE).

The boiling tests were performed by using HFE-7100 (3M™ Novec™) at saturation conditions. As a reference surface, it was tested a plain surface (R_a = 0.14 µm) obtained by using the polishing method presented by Manetti et al. (2017). Vacuum was created to feed the chamber with the working fluid. Before each run, the auxiliary heater boiled the working fluid during 1 hour for degassing it. The test conditions were adjusted by monitoring the pressure and the temperature inside the boiling chamber. For each metal foam test, the experiment was carried out at least twice under similar conditions to ensure that the results were repeatable.

A data acquisition system (Agilent 34970A) acquired all data signals (voltage, pressure, and temperature). The applied heat flux was compared to the measured heat flux by using the Fourrier's law of conduction through the three thermocouples in the copper block,

$$q''_{measured} = \frac{\pi}{4} \cdot k_{Cu} \cdot \frac{\Delta T_{13}}{L_{13}} \tag{3}$$

where π/4 is due to the square cross section at the surface upper level; L_{13} is the thermocouples distance (12 mm).

The HTC was calculated using Newton's law of cooling given by:

$$h = \frac{q''_{measured}}{T_w - T_{sat}\,(p_{int})} = \frac{q''_{measured}}{\Delta T_{sat}} \tag{4}$$

where $T_{sat}(p_{int})$ corresponds to the saturation temperature of the HFE-7100 at pressure inside de boiling chamber that is given by (3M Company, 2002), and T_w is the wall temperature given as follows:

$$T_w = T_1 - \frac{q''_{measured}}{k_{Cu}} \cdot \frac{4}{\pi} L_{1s} - \frac{q''_{measured}}{k_{Cu}} \cdot L_{sw} \tag{5}$$

where the second term is the linear temperature profile at the end of circular section (L_{1s} = 5 mm) and the third term is the linear temperature profile in the square section (L_{sw} = 3 mm) as shown Fig. 5b.

The experimental uncertainties were calculated by using the method described by Moffat (1988). The experimental uncertainty of the heat transfer coefficient is higher for low heat fluxes, decreasing as heat fluxes increase. For all surfaces tested, the experimental uncertainty for the heat flux and the heat transfer coefficient varied from 18.3 to 3.3 % and from 18.4 to 3.8 %, respectively.

4. Results and Discussion

4.1 Validation of the experimental apparatus

In order to verify the pool boiling apparatus accuracy, tests were carried out for HFE-7100 on the plain surface comparing them with the predictions values based on well-known correlations from literature (Fig. 6): Rohsenow's correlation (1952), Cooper (1984), Ribatski and Jabardo (2003) and the Stephan's fitting (1992), and also, Kiyomura et al. (2017).

The predicted values agree well with the experimental data with a mean absolute percentage error (MAPE) of 11% for Rohsenow's correlation by using a C_{sf} = 0.00316, based on Priarone (2005), and 12% for Kiyomura et al. (2017) correlation by using the static contact angle, θ = 2°. Cooper's correlation presents a MAPE of 26% and, Ribatski and Jabardo correlation presents the lowest error, equal to 10.6%. The exponent n obtained by Stephan's fitting was around 0.7, agreeing with the value that generally lies between 0.6 and 0.8.

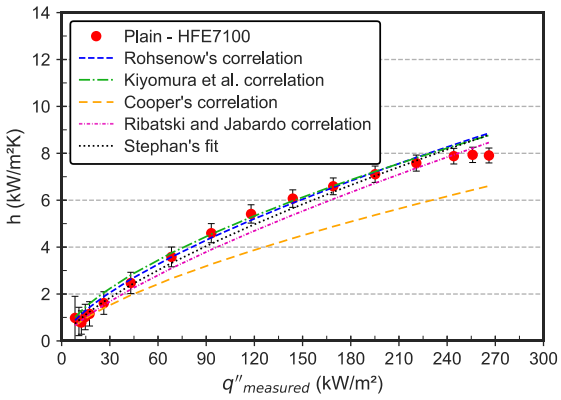

Figure 6. Pool boiling apparatus validation with HFE-7100.

4.2 Copper foams pool boiling curves

The boiling curves for metal foams and plain surface are shown in Fig. 7 and, Fig. 8a shows the HTC curves. In the plain surface the sites remain non-actives until a heat flux of 15 kW/m² and superheating higher than 15 °C were attained; meanwhile, the copper metal foam eliminated the thermal overshoot at the onset nucleate boiling (ONB), with some nucleation sites being activated at the first heat fluxes (≈10 kW/m²).

For q'' < 50 kW/m², foams with δ = 2 mm and δ = 3 mm showed no significant difference between them. In this way, even that copper has a high thermal conductivity (k_{Cu} ≈ 400 W/m.K) and the foam with higher thickness has greater wet area, the temperature drop through the copper foam plays a key role in the first heat fluxes and, then, foams with thickness higher than 2 mm is not useful for heat transfer. Moreover, 'Cu foam 1 mm' presented the worst performance due to the lowest wet area. Therefore, even that all foams showed active sites at first heat fluxes, the natural convection also plays a role for heat fluxes up to 50 kW/m², affecting the foams boiling curve.

As the heat flux increased, the thickness effect became more evident. In the heat flux range of 50 kW/m² < q'' < 200 kW/m², corresponding to fully developed nucleate boiling regime, the 'Cu foam 2 mm' presented better heat transfer performance than 'Cu foam 3 mm'; for heat flux higher than 200 kW/m², the foam with δ = 1 mm presented the highest HTC as compared to the other surfaces.

In order to show more clearly the HTC enhancement effect of the foams, the experimental results were evaluated by using the heat transfer enhancement ratio, which is given by the ratio between the foam HTC and plain HTC as shown Fig. 8b.

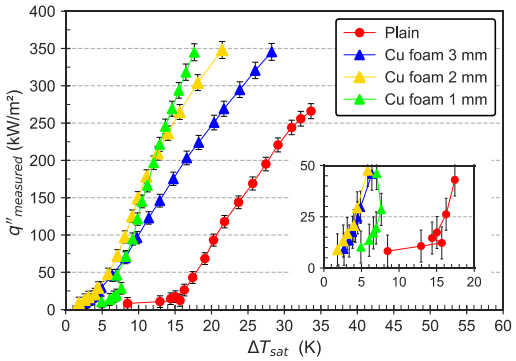

Figure 7. HFE-7100 pool boiling on copper foams at saturation conditions.

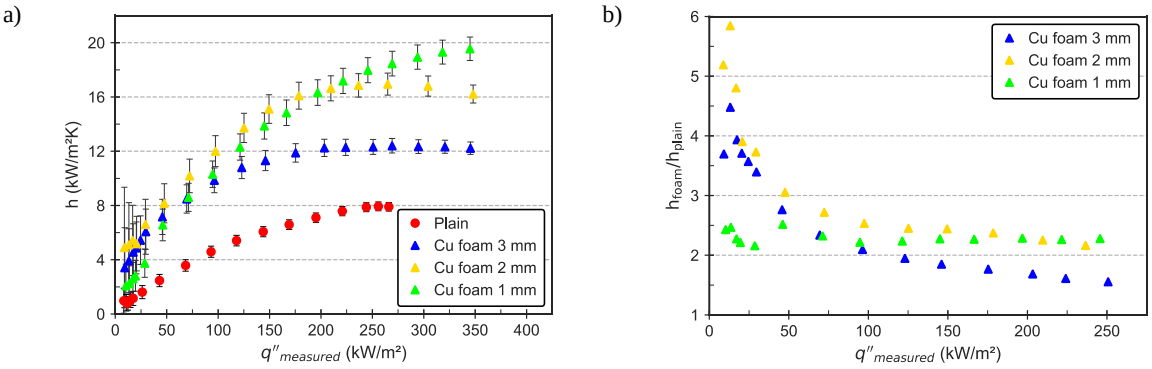

Figure 8. (a) HTC curves for HFE-7100 at saturation conditions and (b) Pool boiling heat transfer coefficient enhancement ratio as a function of heat flux.

Figure 8b confirms the best performance of δ = 1 mm, maintaining an enhancement ratio almost constant close to 2.3, which corresponds to a 130% increase in the HTC. As the dryout heat flux for the plain surface was close to 250 kW/m² and the maximum heat flux applied was 270 kW/m², the HTC ratio analysis was not carried out for the entire foam curves.

For q'' > 200 kW/m², the bubble frequency and coalescence increase within the foam structure. Thus, the higher the foam thickness the higher the bubble evacuation resistance; the vapor bubbles are trapped in the foam structure, leading to an unstable boiling pattern which inhibits the cooling effect and increases the wall temperature. Therefore, the lowest thickness showed the best result at high heat fluxes because even though the wet area decreased, two other effects are pronounced: the vapor bubbles grow and rise easily and, the wickability effect increases, *i.e.*, it has large capability for pumping liquid to the hotspots. Figure 9a shows the maximum HTC for the foams tested compared to the plain surface; and, Fig. 9b shows the dryout heat flux for the foams compared to the plain surface. One may observe that 'Cu foam 1

mm' has the best performance when critical/turning points are compared on both analysis; on the other hand, 'Cu foam 2 mm' is able to reach a high HTC however, the dryout heat flux is close to the 'Cu foam 3 mm' and the plain surface.

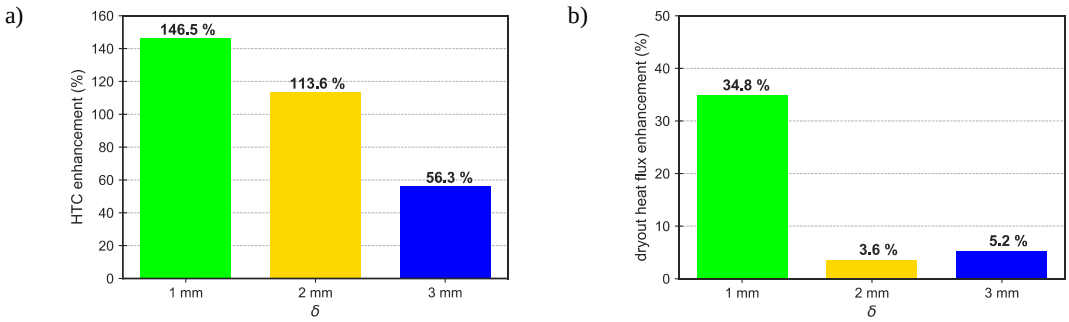

Figure 9. (a) Maximum HTC enhancement for Cu foam; (b) dryout heat flux for Cu foam.

In order to obtain an optimum thickness as a function of heat flux, the results were plotted as a function of the foam thickness at constant heat flux lines as shown in Fig. 10. The minimum superheating value and the maximum HTC value were found by fitting a second-degree polynomial curve with a least-square method with $R^2 > 0.99$.

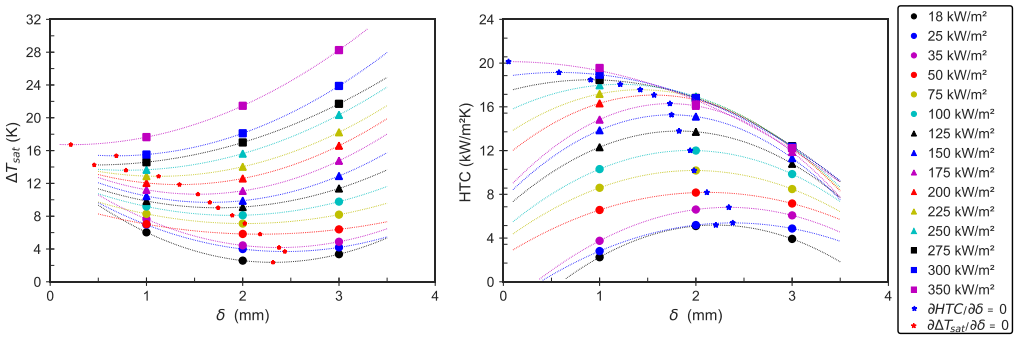

(a) (b)

Figure 10. Copper foam thickness variation: (a) Minimum superheating; (b) Maximum HTC.

The optimum thickness varies with heat fluxes and Fig. 11 shows the turning point for each heat flux. From maximum and minimum points, an inverse S-shaped curve,

$$\delta_{opt} = \frac{a}{b + \exp(c \cdot q'' - d)} \tag{8}$$

was fitted to find the optimum thickness, δ_{opt}, as shown in Fig. 11.

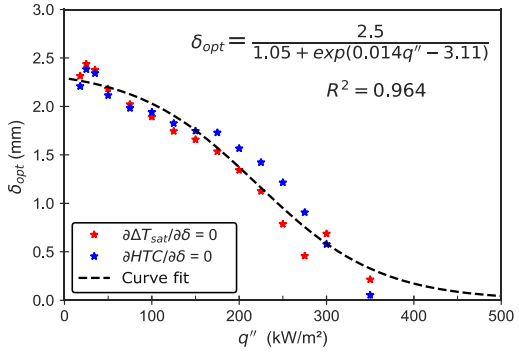

Figure 11. Copper foam optimum thickness for HFE-7100.

It is worth mentioning that the equation obtained in Fig. 11 is valid for metal foams with similar characteristics. However, the inverse S-shaped curve model proved to be a good option for this analysis because: i) it fits a maximum thickness at low heat fluxes where the larger wet area combined with the natural convection plays a key role; ii) it shows the point where the vapor bubbles start to get trapped in the foam cell; and, iii) it presents a minimum foam thickness higher than 0, since 0 means a plain surface where the boiling performance is worst. In our study, the optimum thickness for heat fluxes in the rage of 25 to 100 kW/m² is close to 2 mm, corroborating the inactive area for

higher thickness as reported previously. For q'' > 100 kW/m², the optimum thickness decreases to values lower than 2 mm due to the trapped effect of the vapor bubbles.

4.3 Vapor bubble dynamic visualization

Bubbles dynamics were visualized by using a high-speed camera (Photron FASTCAM SA3) with 1024 × 1024 maximum resolution and 1000 fps. Through videos and image tracking software, the bubble departure diameter (D_d) was calculated by averaging three diameter measurements immediately after the instant time that the bubble detached from the surface, as explained by Thiagarajan et al. (2015); for each heat flux the diameters were measured at least three different sites during 1 second of recording. Then, the arithmetic average diameters of all the evaluated bubbles for a certain experimental condition were calculated. For the highest foam thickness, small bubbles grow and coalescence within the foam structure leading to the bubble departure diameter bigger than the other foams and plain surface. Such behavior decreases as the thickness also decreases for δ = 2 mm and δ = 1 mm. Figure 12 shows the bubbles images and Fig. 13 presents a schematic drawing in order to improve the discussion.

Plain	Cu foam 3 mm	Cu foam 2 mm	Cu foam 1 mm
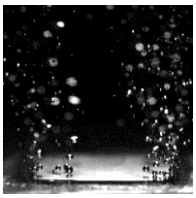	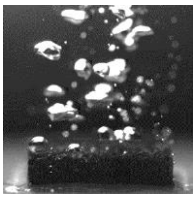	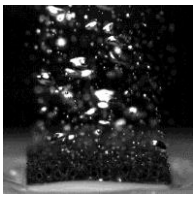	
ΔT_{sat} =14.4 K D_d = 0.7 mm	ΔT_{sat} = 3.8 K D_d =1.9 mm	ΔT_{sat} = 3.1 K D_d =1.8 mm	ΔT_{sat} = 6.6 K D_d =1.2 mm

Figure 12. Vapor bubbles visualization at low heat flux for plain surface and foams.

a) b)

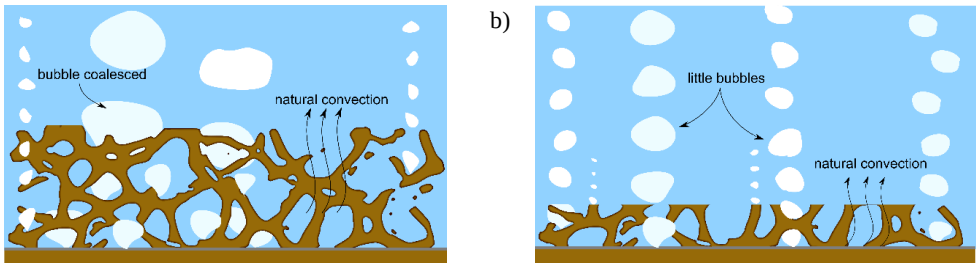

Figure 13. Schematic drawing of vapor bubble dynamics at low heat fluxes on copper foams with thickness of (a) 3 mm and (b) 1 mm.

The coalescence of the vapor bubbles makes measurements above 25 kW/m² difficult and not reliable; however, it is possible to compare the vapor bubbles patterns. Figure 14 shows vapor bubbles visualization at different heat flux. For the highest foam thickness, the bubbles flow not only through the foam upper surface but also through its lateral sides, blocking the liquid-vapor counter-flow and decreasing the HTC.

Cu foam 3 mm	Cu foam 2 mm	Cu foam 1 mm
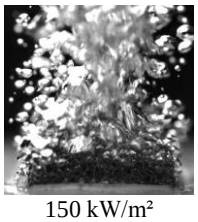	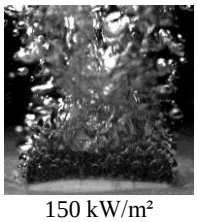	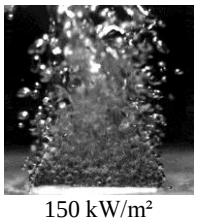
150 kW/m² ΔT_{sat} = 12.9 K	150 kW/m² ΔT_{sat} = 9.9 K	150 kW/m² ΔT_{sat} = 10.5 K
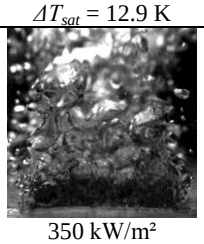	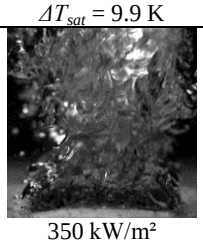	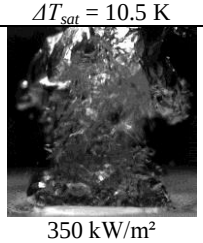
350 kW/m² ΔT_{sat} = 28.3 K	350 kW/m² ΔT_{sat} = 21.5 K	350 kW/m² ΔT_{sat} = 17.6 K

Figure 14. Vapor bubbles pattern at different heat flux values.

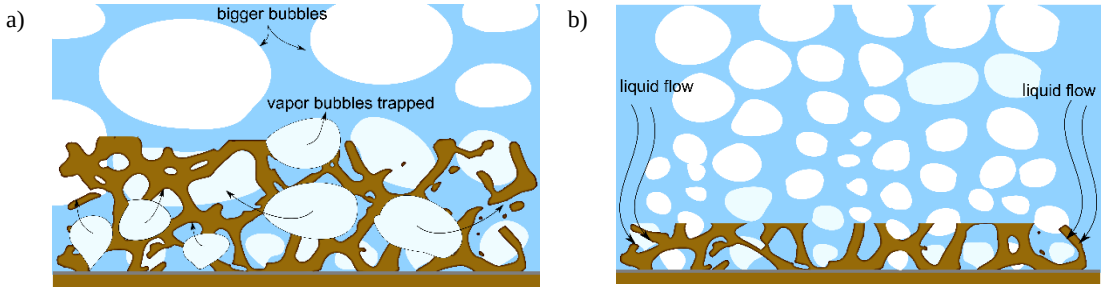

Figure 15. Schematic drawing of vapor bubble dynamics at high heat fluxes on copper foams with thickness of (a) 3 mm and (b) 1 mm.

4.4 Summary of thickness foam influence on pool boiling

By analyzing the foam thickness effect on pool boiling of HFE-7100, one may observe that there is an optimum thickness value at low heat fluxes, close to 2 mm, which eliminates the ONB overshoot and improves the HTC due to the bubbles nucleation and natural convection heat transfer. Highest thickness has useless area for heat transfer due to the temperature drop while lowest thickness has smallest area that influences mainly in the natural convection heat transfer. Moreover, the nucleation sites and bubble frequency increase as heat flux increases, leading to the entrapment of the vapor bubbles in the foam cell, which inhibits the liquid flow into the foam structure and, consequently, deteriorates the HTC. Therefore, lowest foam thickness reduces the entrapment of the vapor in the cell structure, and also, it increases the capillary-wicking ability, which improves the HTC and the dryout heat flux (improves the liquid replenishment in the foam cell delaying the dryout occurrence).

5. CONCLUSIONS

In this work, we presented a pool boiling experimental work by using HFE-7100, at saturated conditions, and copper foams with thickness of 1 mm, 2 mm, and 3 mm as heating surfaces. The following conclusions can be drawn:

- ✓ The copper foams eliminate the thermal overshoot at the onset nucleate boiling, with some nucleation sites being activated at low heat fluxes values. Moreover, these heating surfaces improve the HTC due to the latent heat coupled with natural convection heat transfer.
- ✓ For heat fluxes lower than 200 kW/m², the 'Cu foam 2 mm' has the highest HTC; for heat fluxes higher than 200 kW/m², the 'Cu foam 1 mm' has the best heat transfer performance (an increase of 145% in the HTC as compared to the plain surface).
- ✓ The optimum thickness value varies with the heat flux. In addition, the inverse S-shaped curve fits well with the experimental data and it proved to be a good option for this kind of analysis.
- ✓ For the highest foam thickness, small vapor bubbles grow and coalescence within the foam structure leading to a bubble departure diameter bigger than the other foams and plain surface. Moreover, the bubbles flow not only through the foam upper surface but also through its lateral sides, blocking the liquid-vapor counter-flow and decreasing the HTC.
- ✓ The capillary-wicking ability increases as the foam thickness decreases, improving the HTC and the liquid replenishment in the foam cell delaying the dryout occurrence.

6. ACKNOWLEDGMENTS

The authors are grateful for the financial support from the PPGEM – UNESP/FEIS, from CAPES, from CNPq (CNPq grant number 458702/2014-5) and from FAPESP (grant number 2013/15431-7; 2017/13813-0). Their also extend their gratitude to Prof. Dr. Alessandro Roger Rodrigues and Prof. Dr. Tito José Bonagamba (Escola de Engenharia de São Carlos/EESC-USP) for their important contribution to this work.

7. REFERENCES

3M product brochure, 3M Novec™ engineered fluid HFE-7100 for heat transfer, (2002).

3M product information, Fluorinert™ Eletronic Liquid FC-72, (2000).

Ahn, H. S., Park, G., Kim, J. M., Kim, J., and Kim, M. H., 2012. "The effect of water absorption on critical heat flux enhancement during pool boiling". *Experimental Thermal and Fluid Science*, Vol. 42, pp. 187-195.

Ashby, M. F., Evans, T., Fleck, N. A., Hutchinson, J. W., Wadley, H. N. G. and Gibson L. J., 2008. *Metal foams: a design guide*.

Athreya, B., Mahajan, R., and Sett, S.,2002. "Pool boiling of FC-72 over metal foams: effect of foam orientation and geometry". In *8th AIAA/ASME Joint Thermophysics and Heat Transfer Conference*, St.Louis, Missouri-US.

Banhart, J., 2001. "Manufacture, characterisation and application of cellular metals and metal foams". *Progress in materials science*, Vol.46, No. 6, pp.559-632.

Brun, E., Vicente, J., Topin, F., and Occelli, R., 2008. "IMorph: A 3D morphological tool to fully analyse all kind of cellular materials". *Cellular Metals for Structural and Functional Applications*.

Cao, Z., Liu, B., Preger, C., Wu, Z., Zhang, Y., Wang, X., and Sundén, B., 2018. "Pool boiling heat transfer of FC-72 on pin-fin silicon surfaces with nanoparticle deposition". *International Journal of Heat and Mass Transfer*, Vol. 126, pp.1019-1033.

Cao, Z., Wu, Z., Pham, A. D., Yang, Y., Abbood, S., Falkman, P., and Sundén, B., 2019. "Pool boiling of HFE-7200 on nanoparticle-coating surfaces: Experiments and heat transfer analysis". *International Journal of Heat and Mass Transfer*, Vol. 133, pp. 548-560.

Cooper, M. G.,1984. "Heat flow rates in saturated nucleate pool boiling-a wide-ranging examination using reduced properties". In *Advances in heat transfer*, Elsevier, Vol. 16, pp. 157-239

El-Genk, M. S., 2012. Immersion cooling nucleate boiling of high power computer chips. *Energy conversion and management*, Vol. *53* No. 1, pp. 205-218.

El-Genk, M. S., and Parker, J. L., 2008. "Nucleate boiling of FC-72 and HFE-7100 on porous graphite at different orientations and liquid subcooling". *Energy conversion and management*, Vol. 49, No. 4, pp. 733-750.

Gibson, L.J. and Ashby, M. F., 1997. *Cellular Solids: Structure and properties.* Cambridge Solid State Science Series, 2nd edition, Cambridge University Press.

Groover, M. P.,2012. *Fundamentals of modern manufacturing: materials processes, and systems*. John Wiley & Sons, 5th edition.

Khan, S. A., Sezer, N., and Koç, M., 2019. "Design, fabrication and nucleate pool-boiling heat transfer performance of hybrid micro-nano scale 2-D modulated porous surfaces". *Applied Thermal Engineering*, Vol. 153, pp. 168-180.

Kiyomura, I. S., Mogaji, T. S., Manetti, L. L., and Cardoso, E. M., 2017. "A predictive model for confined and unconfined nucleate boiling heat transfer coefficient". *Applied Thermal Engineering*, Vol. 127, pp. 1274-1284.

Leong, K. C., Ho, J. Y., and Wong, K. K., 2017. "A critical review of pool and flow boiling heat transfer of dielectric fluids on enhanced surfaces". *Applied Thermal Engineering*, Vol. *112*, pp. 999-1019.

Liang, G., and Mudawar, I, 2019. Review of pool boiling enhancement by surface modification. *International Journal of Heat and Mass Transfer*, Vol. 128, pp. 892-933.

Lin, L., and Kedzierski, M. A., 2019. "Review of low-GWP refrigerant pool boiling heat transfer on enhanced surfaces". *International journal of heat and mass transfer*, Vol.131, pp.1279-1303.

Manetti, L. L., Stephen, M. T., Beck, P. A., and Cardoso, E. M., 2017. "Evaluation of the heat transfer enhancement during pool boiling using low concentrations of Al_2O_3-water based nanofluid". *Experimental Thermal and Fluid Science*, Vol. 87, pp. 191-200.

Moffat, R. J., 1988. "Describing the uncertainties in experimental results". *Experimental thermal and fluid science*, Vol 1, pp. 3-17.

Priarone, A., 2005. "Effect of surface orientation on nucleate boiling and critical heat flux of dielectric fluids". *International journal of thermal sciences*, Vol. 44, No. 9, pp. 822-831.

Rahman, M. M., Olceroglu, E., and McCarthy, M., 2014. "Role of wickability on the critical heat flux of structured superhydrophilic surfaces". *Langmuir*, Vol. 30, No. 37, pp. 11225-11234.

Ribatski, G., and Jabardo, J. M. S., 2003. "Experimental study of nucleate boiling of halocarbon refrigerants on cylindrical surfaces". *International journal of heat and mass transfer*, Vol. 46, No. 23, pp. 4439-4451.

Rohsenow, W. M., 1952. "A method of correlating heat transfer data for surface boiling of liquids". *Transactions of ASME – J. Heat Transfer*, Vol. 74, pp. 969-97.

Sarangi, S., Weibel, J. A., and Garimella, S. V., 2017. "Quantitative evaluation of the dependence of pool boiling heat transfer enhancement on sintered particle coating characteristics". *Journal of Heat Transfer*, Vol.139, No. 2, 021502.

Seo, H., Lim, Y., Shin, H., and Bang, I. C., 2018. "Effects of hole patterns on surface temperature distributions in pool boiling". *International Journal of Heat and Mass Transfer*, Vol. 120, pp. 587-596.

Shojaeian, M., and Koşar, A., 2015. "Pool boiling and flow boiling on micro-and nanostructured surfaces". *Experimental Thermal and Fluid Science*, Vol.63, pp.45-73.

Stephan, K., 1992. *Heat transfer in condensation and boiling*. Springer-Verlag.

Teodori, E., Moita, A. and Moreira, A., 2014. "Empirical and modelling based correlations for pool boiling over micro-structured surfaces". *Interfacial Phenomena and Heat Transfer*. Vol. 2 No. 3, pp. 273-292.

Thiagarajan, S. J., Yang, R., King, C., and Narumanchi, S., 2015. "Bubble dynamics and nucleate pool boiling heat transfer on microporous copper surfaces". *International Journal of Heat and Mass Transfer*, Vol. 89, pp.1297-1315.

Vicente, J., Topin, F., and Daurelle, J. V., 2006. "Open celled material structural properties measurement: from morphology to transport properties". *Materials transactions*, Vol.47. No. 9, pp.2195-2202.

Wong, K. K., and Leong, K. C., 2018. "Saturated pool boiling enhancement using porous lattice structures produced by Selective Laser Melting". *International Journal of Heat and Mass Transfer*, Vol.121, pp.46-63.

Xu, J., Ji, X., Zhang, W., and Liu, G., 2008. "Pool boiling heat transfer of ultra-light copper foam with open cells". *International Journal of Multiphase Flow*, Vol. 34, No. 11, pp.1008-1022.

Xu, Z. G., and Zhao, C. Y., 2013. "Thickness effect on pool boiling heat transfer of trapezoid-shaped copper foam fins". *Applied Thermal Engineering*, Vol.60, No. 1-2, pp.359-370.

Xu, Z. G., and Zhao, C. Y., 2015. "Experimental study on pool boiling heat transfer in gradient metal foams". *International Journal of Heat and Mass Transfer*, Vol.85, pp.824-829.

Yang, X. H., and Liu, J., 2018. "Advances in Liquid Metal Science and Technology in Chip Cooling and Thermal Management". *Advances in Heat Transfer*, Elsevier, Vol. 50.

Yang, Y., Ji, X., and Xu, J., 2010. "Pool boiling heat transfer on copper foam covers with water as working fluid". *International Journal of Thermal Sciences*, Vol. 49, No. 7, pp.1227-1237.

Zhao, C. Y., 2012., "Review on thermal transport in high porosity cellular metal foams with open cells". *International Journal of Heat and Mass Transfer*, Vol. 55, No. 13-14, pp.3618-3632.

Zhou, L., Li, W., Ma, T., and Du, X., 2018. "Experimental study on boiling heat transfer of a self-rewetting fluid on copper foams with pore-density gradient structures". *International Journal of Heat and Mass Transfer*, Vol.124, pp.210-219.

8. RESPONSIBILITY NOTICE

The authors are the only responsible for the printed material included in this paper.